analytical chemistry

pubs.acs.org/ac Article

Well-Orientation Strategy for Direct Immobilization of Antibodies: Development of the Immunosensor Using the Boronic Acid-Modified Magnetic Graphene Nanoribbons for Ultrasensitive Detection of Lymphoma Cancer Cells

Pegah Hashemi, Abbas Afkhami, Behzad Baradaran, Raheleh Halabian, Tayyebeh Madrakian, Fabiana Arduini, Tien Anh Nguyen, and Hasan Bagheri*

Cite This: *Anal. Chem.* 2020, 92, 11405−11412 Read Online

ACCESS | Metrics & More | Article Recommendations | Supporting Information

ABSTRACT: This work presents an effective strategy for the well-oriented immobilization of antibodies in which boronic acid is directly attached to the surface and with no need of the long and flexible spacer. A magnetic graphene nanoribbon−boronic-acid-based immunosensor was developed and tested for the impedimetric detection of lymphoma cancer cells, a blood cancer biomarker. Magnetic graphene nanoribbons (MGNRs) were modified with boronic acid (BA) to create a supporting matrix that is utilized by immobilizing anti-CD20 antibodies with good orientation. The prepared biosensing layer (MGNR/BA/Ab) with well-oriented antibodies was premixed into whole blood samples to interact with lymphoma cancer cell receptors. In the presence of target cell receptors, an immunocomplex was formed between anti-CD20 antibodies and lymphoma cancer cell receptors. Then, the biosensing layer was magnetically collected on a screen-printed carbon electrode (SPCE) and placed in a homemade electrochemical cell configuration to measure impedimetric signals. The fabrication steps of the immunosensor were characterized by various techniques, such as resonance light scattering, fluorescence, electrochemical impedance spectroscopy, and cyclic voltammetry. The assay is highly sensitive: the calculated limit of detection of lymphoma cancer cells was as low as 38 cells/mL, and the detection was linear from 100 to 1 000 000 cells/mL. The specificity of the immunosensor is also very high, and there is no interference effect with several potential interferents, such as the breast cancer (MCF-7), human embryonic kidney (HEK293), and leukemia (HL-60 and KCL-22) cell lines. The performance of the immunosensor for lymphoma cancer cells in clinical blood samples is consistent with that of commercial flow cytometric assays.

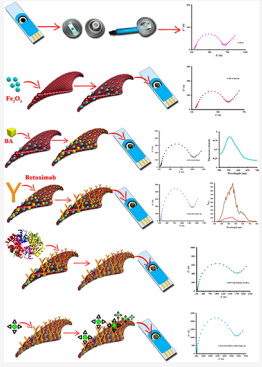

Cancer is the second most common cause of death worldwide, presenting a major and unmet challenge to healthcare globally.[1] Early tumor diagnosis is essential for the effective and ultimately successful treatment of cancers. It has been reported that characterization of the antigen surface properties of a cancer cell is essential for understanding the disease and developing targeted therapy.[2] CD20 is a B-cell-specific antigen[3] that is expressed on mature B cells and in most non-Hodgkin's lymphomas but not on early progenitors or later mature plasma cells.[4] This nonglycosylated 33 to 37 kDa phosphoprotein is expressed on more than 90% of B cell lymphomas and is a B cell surface protein with the capacity to serve as a calcium channel, initiate intracellular signals, and modulate cell growth and differentiation.[5,6] It is also an attractive target for antibody (Ab) therapy for the treatment of non-Hodgkin's lymphoma (NHL)[2] and B cell chronic lymphocytic leukemia (B-CLL).[7] Rituximab (Rituxan), a chimeric murine/human-engineered monoclonal anti-CD20 Ab,[2,7,8] is a monoclonal Ab directed against the CD20 antigen.[3] Monoclonal Ab therapy with rituximab represents one of the most important advances in the treatment of lymphoproliferative disorders in the past 30 years.[9]

The most recent efforts in cancer cell detection have focused on the development of biosensors with adequate sensitivity and selectivity, rapid detection, and easy operation.[10] Biosensors that utilize protein−protein interactions have emerged as an attractive topic for improving our understanding of biorecognition processes for drug discovery, clinical diagnostics, and cancer therapy.[11] Among various types of electrochemical affinity biosensors, electrochemical immunosensors based on specific antigen−antibody interactions are the most widely used due to some of their unusual features.[12] An efficient strategy for the Ab immobilization is firmly needed to succeed, in order to sensitively detect a specific target

Received: June 2, 2020
Accepted: July 20, 2020
Published: July 20, 2020

https://dx.doi.org/10.1021/acs.analchem.0c02357
Anal. Chem. 2020, 92, 11405−11412

biomolecule.[13] The stability and accessibility of a surface-bound protein's active site may be influenced significantly by the orientation of the protein on the solid support.[14] To fully retain biological activity, antibodies should be attached to surfaces without affecting conformation and function. The available protocols for Ab immobilization can be categorized into two groups: oriented/site-specific and random immobilizations. In some cases, immobilization may lead to partial or even complete loss of protein activity because of random orientation and structural deformation.[15,16] Hence, novel strategies presenting appropriate orientation of the immobilized Abs under a simple process are essentially required to accomplish the needs for highly sensitive and reproducible measurements.[13]

Strategies for oriented Ab immobilization with the target of attaching the Ab to the sensing layer surface via its Fc region, far away from the binding sites.[15] It was concluded that boronic acid (BA) forms the stable complex with the mono- and oligosaccharides.[13] BA rapidly and reversibly forms cyclic boronate esters with cis-diols in both nonaqueous and aqueous milieus.[14] It has been confirmed that on account of the high number of pendant groups in the chains, BA-containing materials are able to interact with their biological receptors in a multivalent way, causing the high increase of the affinity and specificity of the biomimetic binding.[13] Because the carbohydrate region is located in the Fc domain, which is not involved in antigen-binding activity, interactions between BA and the carbohydrate chains are unlikely to affect the biological activity of the immobilized Abs.[14] However, only a few works have reported the oriented immobilization strategy of antibodies for the immunoassays by boronate formation mechanism.[13]

As mentioned before, immobilization strategy is not simple enough. The N-glycans are nestled between the Ab Fc chains, and quite far from the C-terminus/"bottom." In the absence of a spacer or even using too short spacers for the attachment of BA to the surface could compel Ab to "lie" on the surface or prevent its immobilization. This would not be optimal for the complete bound of the antigen. In the case of a spacer with appropriate properties such as proper length and flexibility, it puts the BA far from the surface. Under this condition, the Ab has the stand position for the optimal interactions with antigens.[15] Therefore, applying the spacer with an appropriate length can help to succeed in Ab immobilization.

Carbon nanomaterial surfaces can be further modified via the oxygen-containing functional groups of carbon structures for better solubility, biocompatibility, and multifunctionality.[17] Graphene nanoribbons (GNRs) are strips of graphene with a high length-to-width ratio and straight edges.[18] The high surface area of GNRs makes them ideal fillers for nanocomposites materials.

Two top-down synthesis approaches have been widely explored for the fabrication of GNRs. The first approach is based on the cutting or etching of graphene or graphite precursors into narrow stripes, while the second approach is the longitudinal unzipping of carbon nanotubes (CNTs).[19] In the second approach, the properties of the precursor are crucial for further processing of the resulting GNRs in electronic devices. Therefore, multiwalled carbon nanotubes (MWCNTs) with diameters between 40 and 80 nm and high solubility in water and polar organic solvents have been used as alternative precursors. This is a simple, efficient, and potentially scalable technique for making quasi-GNRs in solution.[20]

In this study, by taking advantage of the rituximab monoclonal anti-CD20 Ab, which specifically binds to the B cell membrane surface, we introduced a strategy for the specific detection of lymphoma cancer cells. For this purpose, we developed a label-free impedimetric immunosensor. Synthesized magnetic graphene nanoribbons (MGNRs) were modified with BA, and Ab was immobilized on MGNR/BA. After the interaction of MGNR/BA/Ab with cancer cells, the modified nanocomposite was magnetically collected on a screen-printed carbon electrode (SPCE) and placed in a homemade electrochemical cell, and impedance signals were recorded. The main parameters affecting the immunosensor performance were optimized. Different modification steps of the nanocomposite were characterized by various techniques, such as resonance light scattering (RLS), fluorescence, electrochemical impedance spectroscopy (EIS) and cyclic voltammetry. Finally, the optimized procedure was employed for the detection and determination of cancer cells in real samples.

EXPERIMENTAL SECTION

Reagents. The details of this section are described in the Supporting Information.

Instrumentation. The details of this section are described in the Supporting Information

Preparation of GNR, MGNRs, MGNR/BA, and MGNR/BA/Ab. GNRs were synthesized from MWCNTs according to the method reported by Tour et al.[18] The details of this section is described in the Supporting Information.

Magnetic-GNR hybrids have been synthesized according to the simple method reported by Kim et al.[21] The details of this section are described in the Supporting Information. Binding BA was easily achieved by the reaction between carboxylic groups from MGNRs and NH_2 groups of BA. Thus, 0.020 g of synthesized MGNRs was added to 2 mL of EDC (20 mM) and NHS (30 mM) solution and stirred at room temperature for 2 h. After the reaction, the activated MGNRs were isolated from the solution by placing the mixture on a magnet and then rinsed with water. The obtained activated MGNRs were dispersed in 5 mL of DDW. Then, 1.5 mL of the solution was added to an equal volume of 0.1% BA, and the mixture was slowly stirred at room temperature for 2 h. After magnetic isolation and washing with DDW, the obtained MGNR/BA was dispersed in 10 mL of DDW and kept in the refrigerator (4 °C) before use.

To immobilize the Ab on the MGNR/BA surface, 1 μL of Ab (1 mg/mL) was added to 9 μL of MGNR/BA composite suspension (for a final Ab concentration of 100 μg/mL) and gently stirred for 3 min. Then, the mixture was incubated at 4 °C for 4 h. The sample vial was placed on the external magnet, and after accumulation of the MGNR/BA/Ab at the bottom, the solution was removed. The MGNR/BA/Ab was washed with DDW and separated by a magnet.

Finally, the surface of the nanocomposite was blocked by BSA (0.05% w/v) for 1 h to block the possible remaining active sites and avoid nonspecific binding.[16] The fabricated immunoprobe was stored in the refrigerator at 4 °C until use.

Fabrication of the Proposed Immunosensor. The proposed immunosensor fabrication includes several steps, which are shown in Scheme S1. First, 10 μL of prepared immunoprobe suspension was added to equal volumes of different concentrations of B cell lymphoma cancer cells. The mixture was stirred for 2 min and kept for 2.5 h at room

https://dx.doi.org/10.1021/acs.analchem.0c02357
Anal. Chem. 2020, 92, 11405−11412

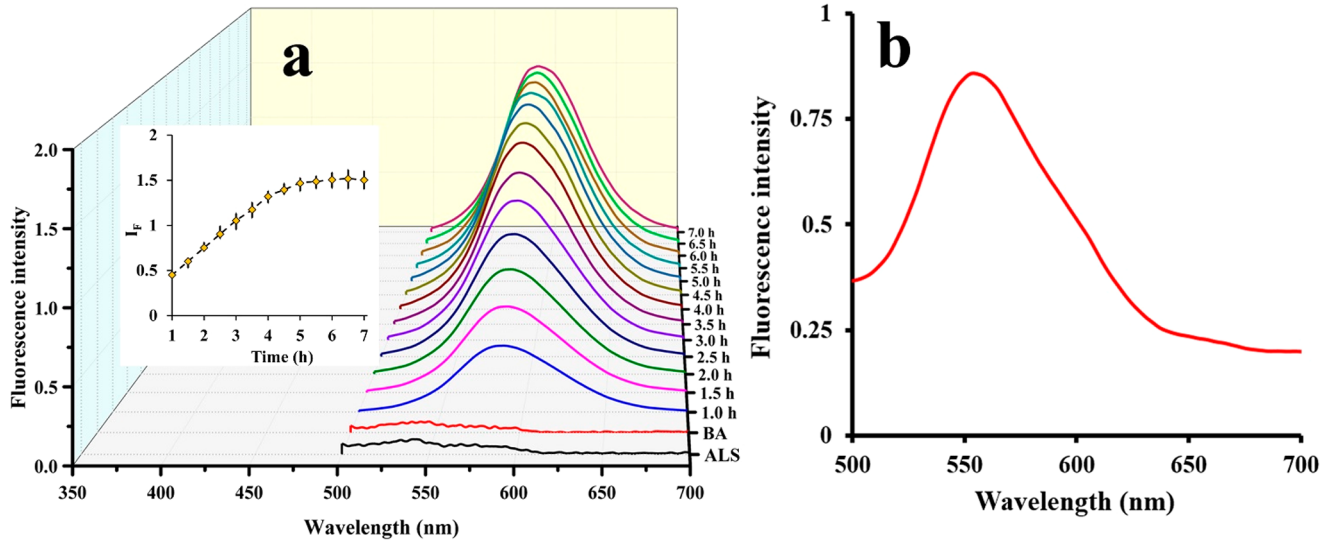

Figure 1. (a) Fluorescence spectra of BA-ARS complex formation in solution at various times. The inset shows the changes in fluorescence intensity at various times (1−7 h). (b) Fluorescence spectrum of the BA-ARS complex on the MGNR surface (MGNR/BA-ARS) at the optimal time of 5 h. The excitation wavelength was 380 nm.

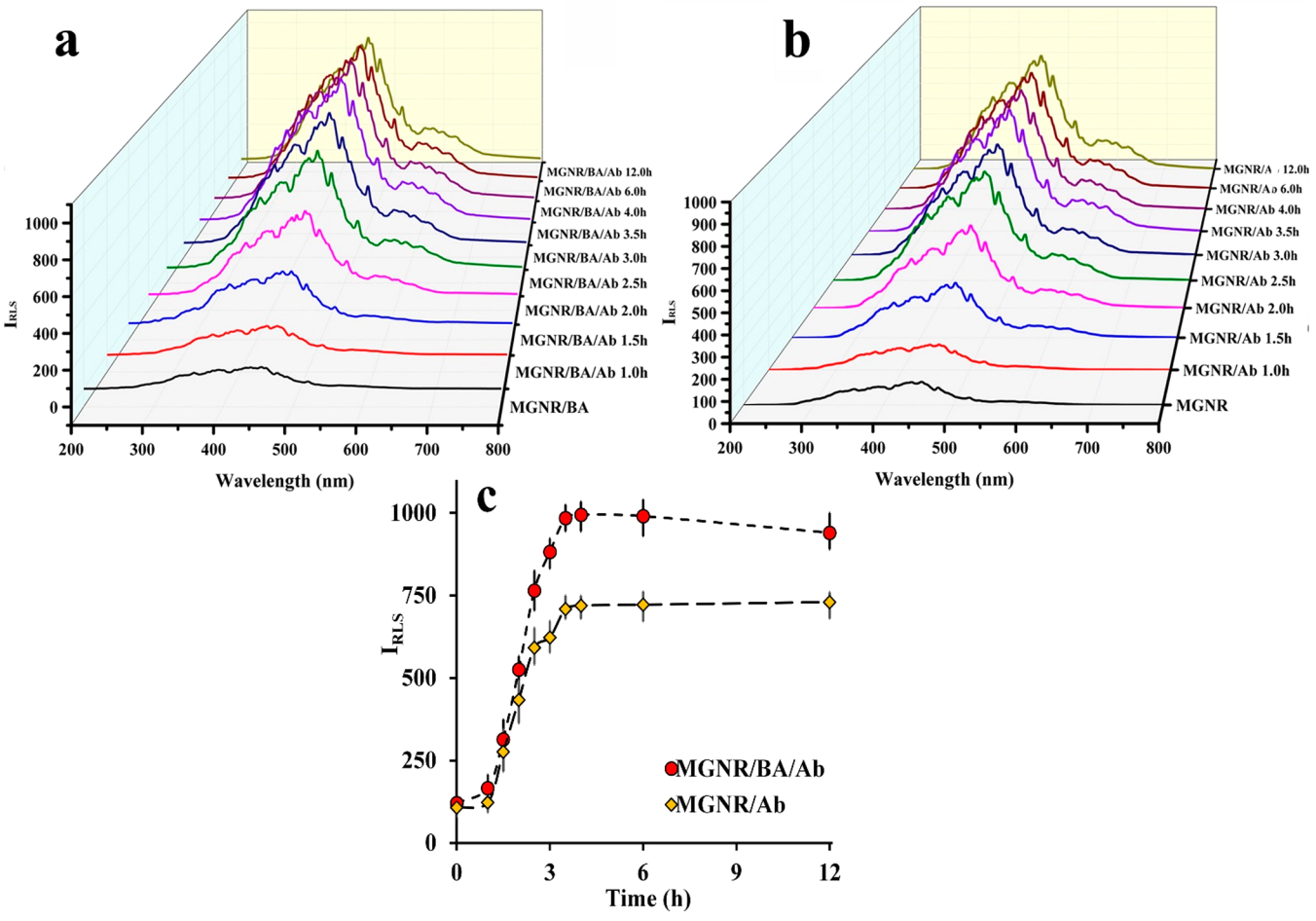

Figure 2. Light scattering spectra of (a) MGNR/BA/Ab and (b) MGNR/Ab at various incubation times. (c) Effect of BA presence on Ab immobilization on the surface at different incubation times. The Ab concentration was 100 μg/mL, and the incubation times were 1, 1.5, 2, 2.5, 3, 3.5, 4, 6, and 12 h.

temperature to allow the reaction to complete. Second, the accumulated B cell lymphoma cancer cells on the magnetic nanocomposite were separated by placement on a magnet. Third, the MGNR/BA/Ab/BSA/cells accumulated at the bottom of the vial, and the supernatant was subsequently removed. To remove the physically adsorbed cells before use,

https://dx.doi.org/10.1021/acs.analchem.0c02357
Anal. Chem. 2020, 92, 11405−11412

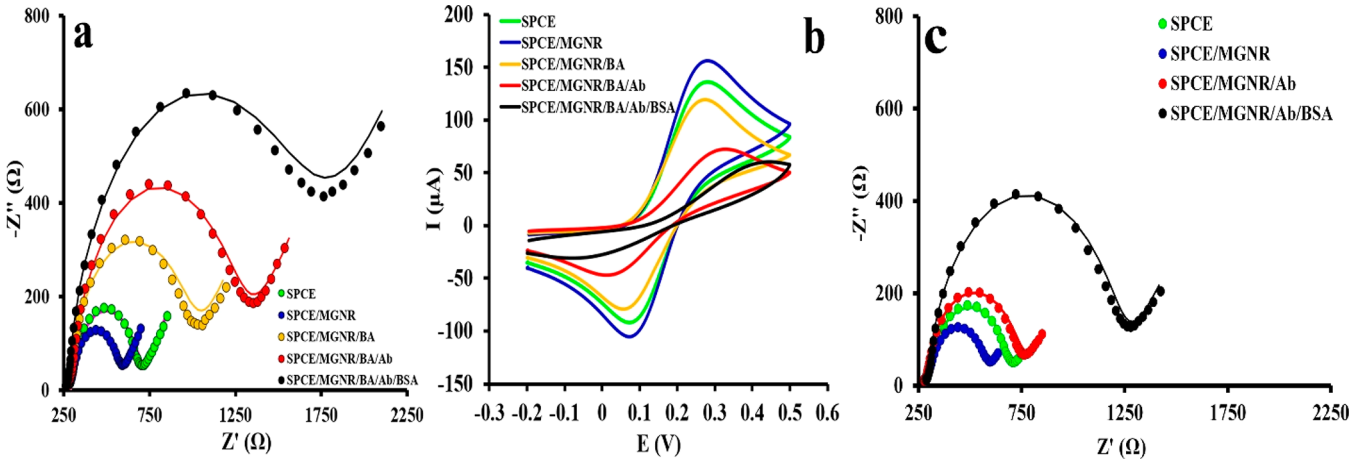

Figure 3. (a) Nyquist plots (dot and line plots related to experimental and fitted data, respectively) and (b) cyclic voltammograms at different MGNR surface modification steps for immunosensor fabrication. (c) Nyquist plots obtained for different MGNR modification steps without the use of BA for Ab immobilization. EIS and CV measurements were carried out in PBS containing KCl (0.1 M) and $[Fe(CN)_6]^{3-/4-}$ (5 mM).

the cell-loaded nanocomposite was washed with DDW. Finally, 10 μL of the cell-loaded nanocomposite was pipetted onto the SPCE surface and placed in a homemade electrochemical cell,[22] and the electrochemical responses were recorded. By placing the magnet below the working electrode surface, the magnetic nanocomposite was captured on the working electrode surface without the need for any complex surface modification steps.[22,23]

Real Sample Preparation. The residuals of two samples (cancer patients) of human whole blood were obtained from a clinical laboratory and used as received without any treatment.[24]

Cell Culture. The details of this section are described in the Supporting Information.

Methylthiazoletetrazolium (MTT) Assay. The details of this section are described in the Supporting Information.

RESULTS AND DISCUSSION

Characterization of the GNRs and MGNRs. GNRs and MGNRs were evaluated using FT-IR, XRD, and TEM. The details of this section are described in the Supporting Information.

Characterization of the MGNR/BA. The intensity of the fluorescence of complexes between BA and Alizarin Red S (ARS) dye, as the fluorescent probe, was measured to precisely characterize the BA conjugation on the MGNR surface.[25] Unlike the dye itself, its complexes with BA exhibit fluorescence.[26] ARS is a dye that specifically couples to BA groups.[27] The binding of a BA to the catechol diol of ARS removes the active protons, which are responsible for greatly quenching the fluorescence of ARS. In other words, the formation of the ARS−PBA complex can greatly increase the fluorescence intensity of ARS.[25] Since ARS does not emit fluorescence itself but can emit intense fluorescence after reacting with BA,[25] the presence of BA on the MGNRs was investigated with ARS as a fluorescent probe.

Fluorescence was measured after mixing the BA solution (0.1%) with the ARS solution (0.1%) at different interaction times from 1 to 7 h. Figure 1a shows the fluorescence emission spectra of the BA-ARS complex at λ_{ex} = 380 nm at different times. The fluorescent emission intensity was relatively constant after 5 h. Therefore, 5 h was selected as the optimum time for formation of the fluorescent complex.

The MGNR/BA was incubated in 0.1% ARS at room temperature for 5 h and rinsed with PBS to remove the unbound ARS dye. The fluorescence spectra of MGNR/BA/ARS shown in Figure 1b revealed that BA was successfully immobilized on the MGNRs and could form a fluorescent complex with ARS.

Characterization of the MGNR/BA/Ab. The Fc regions of Abs are N-glycosylated. Therefore, appropriate orientation of the Ab can be obtained with the immobilization via its N-glycans through the interaction of diols with BA.[15] The immobilization of Ab on the MGNR/BA surface at different incubation times was monitored using the RLS method. RLS has emerged as a powerful optical technique utilizing elastic light scattering and has various advantages, including high sensitivity, rapidness, simplicity, and convenience.[28] The RLS spectra of MGNR/BA/Ab at various incubation times are shown in Figure 2a. The maximum light scattering wavelength of RLS is located at 455 nm. It is clearly shown in the figure that the immobilization of Ab on the MGNR/BA increased the RLS intensity. This is reasonable because the RLS intensity is proportional to r^6, where r is the radius of the particle according to the theory.[28] On the other hand, Ab immobilization leads to an increase in the size of scatter, and the formation of larger complexes causes an increase in the RLS intensities of the system.

The effect of incubation time on the RLS intensity was evaluated for 12 h. Figure 2c shows that a sharp increase after incubation for 4 h leads to an increase in the scattering signal, after which the signal remains relatively constant. This time value was selected as the appropriate optimum value for Ab immobilization on the MGNR/BA surface. The obtained results indicated that Ab was highly immobilized on the MGNR/BA surface at 4 h and stabilized for at least 12 h. These results confirmed that the stability of the proposed immunoprobe (MGNR/BA/Ab) is practical for the construction of immunosensors.

A similar experiment was performed with MGNRs to investigate the role of BA in the immobilization of Abs. The activated MGNRs with EDC/NHS were incubated in Ab solution at different times, and the RLS signal was recorded (see Figure 2b). It is clear that when the incubation time reaches 4 h, the RLS also increases. The obtained results from Figure 2a and b were compared with those in Figure 2c. The

https://dx.doi.org/10.1021/acs.analchem.0c02357
Anal. Chem. 2020, 92, 11405−11412

results indicated that the RLS intensities of MGNR/BA/Ab were greatly enhanced compared with those of MGNR/Ab. These results confirm that the Ab loading was dramatically increased on the MGNR/BA surface compared to the MGNR surface.

Characterization of the Proposed Immunosensor by Electrochemical Methods (EIS and CV). EIS is an electrochemical technique based on analysis of the linear response of the perturbation/response ratio when applied to a low-amplitude sinusoidal perturbation typically ranging from 5−10 mV. It is a powerful tool for the measurement of faradaic processes involving charge transfer between the electrode and some species to be oxidized or reduced in the solution.[29] A redox probe ($[Fe(CN)_6]^{3-/4-}$) can easily participate in the electron transfer kinetics close to the electrochemical double layer. When a biomolecule is immobilized/adsorbed on the electrode surface, it retards the electron transfer rates between the probe and electrochemical double layer. As a result, the charge transfer resistance increases for the redox probe to access the electrochemical double layer.[16]

The R_{CT} was changed for all steps of MGNR modification for immunosensor fabrication. Thus, each MGNR modification step was investigated by EIS to monitor the change in the resistance after each fabrication step of the immunosensor. R_{CT} evaluates the semicircle diameter domain at a higher frequency of the impedance spectra.[22] For accurate estimation of R_{CT} at the electrode surface, an equivalent circuit was used for fitting of the EIS and the obtained results from the Nyquist plot.[30] The impedance spectra were fitted to the modified Randles equivalent circuit composed of the ohmic resistance of the electrolyte solution (R_s) and the charge transfer resistance (R_{CT}), in series with the diffusion-limited Warburg impedance (W) and in parallel to a constant phase element (CPE or Q).[30,31]

Figure 3a illustrates the obtained Nyquist plots from various modification steps of the different impedimetric layers. The line through the data points in Figure 3a demonstrates the fitting curve of the modified Randles equivalent circuit. A good agreement between the fitting curve and the experimental points was observed. The obtained values obtained using fitting are shown in Table 1.

Table 1. Randles Parameters from Figure 4a for the Fabrication Steps of the Proposed Immunosensor

				Q	
electrode	R_s (Ω)	R_{CT} (Ω)	W (mMho)	Y0 (μMho)	N
SPCE	291	401	2.39	2.81	0.883
SPCE/MGNR	290	289	1.69	2.90	0.877
SPCE/MGNR/BA	285	696	0.670	1.69	0.914
SPCE/MGNR/BA/Ab	288	984	0.826	2.29	0.897
SPCE/MGNR/BA/Ab/BSA	272	1370	0.730	8.50	0.902

As shown in Figure 3 and Table 1, the R_{CT} value is 401 Ω when measured with only the SPCE surface. However, it decreases 30% after dropping the MGNRs at the SPCE surface. This result should come from the increase in the nanostructure surface leading to an increase in the electrode current. On the other hand, the R_{CT} resistance increases by approximately 300 Ω after immobilizing Ab on the MGNR surface and dropping on the electrode surface. The formation of the insulating protein layer blocks electron transfer toward the diffusion of the redox probe on the electrode surface, hindering the electron transfer tunnel.[16] The R_{CT} increases more than 3 times after blocking the remaining free spaces on the MGNR/BA/Ab by BSA and dropping on the electrode surface. The result indicates that the modification process was successful.

CV is a useful technique to probe the features of modified electrode surfaces. The changes in peak current along with the peak separation in CVs at various steps of surface modification are theoretically related to the electron transfer rate constant.[30] To study the blocking behavior of various surface modifications, $[Fe(CN)_6]^{3-/4-}$ was used as a redox probe. In our experiment, the results obtained from EIS measurements were confirmed by CV measurements. The cyclic voltammograms corresponding to different modification steps are shown in Figure 3b. Obviously, the large surface of the nanostructure enhances the electron transfer rate on the electrode surface together with a large number of edges, and defects per mass of GNRs can facilitate electron transfer between the probe and the electrode surface.[22] As a result, the anodic peak current (I_{peak}) increased from 91.07 to 109.27, and the peak-to-peak separation (ΔE_{peak}) values decreased from 187.99 to 180.66 after dropping the MGNRs on the SPCE surface. After the addition of MGNR/BA, MGNR/BA/Ab, and MGNR/BA/Ab/BSA to the electrode surface, ΔE_{peak} increased (192.87, 275.88, and 380.86 mV, respectively), and I_{peak} decreased (86.75, 42.87, and 16.06 mA, respectively) due to blocking of the redox probe access to the electrode surface and the difference in the dielectric constants of biological materials and water molecules.[32]

To study the effect of BA on Ab loading, the Nyquist plots corresponding to various MGNR surface modification steps were recorded with and without BA present at the surface. As shown in Figure 3a and c, the obtained R_{CT} from the Ab loading step was increased, and the R_{CT} from the BSA blocking step decreased in the presence of BA. These results demonstrate that, in the absence of BA, the amount of loaded Ab on the ribbon surface was dramatically decreased, leading to an increase in the remaining free spaces on the surface and thus an increase in blocking charge transfer resistance.

Characterization of the magnetic immunoprobe surfaces by scanning electron microscopy (SEM). The details of this section are described in the Supporting Information.

Optimization of Immunoreaction Time. To obtain a satisfactory electrochemical response, the immunoreaction time between the Ab and cancer cells should be optimized.[33,34] Thus, the effect of the immunoreaction time on the impedimetric immunoassay signal was investigated. Furthermore, the immunoreaction time between rituximab and Raji cells was optimized. Figure 4a illustrates the effect of the immunoreaction time between anti-CD20 Ab and Raji cells. The R_{CT} increased sharply during the first hours of incubation and reached a plateau at 2.5 h. This result demonstrated that the effective immunoreaction time between cancer cells and the Ab is 2.5 h. Therefore, this value was chosen as the optimal immunoassay time.

Analytical Performance of the Immunosensor. The electrochemical performance of the proposed biosensor for the Raji cell assay under the optimized conditions was investigated. Figure 4b shows the impedance method and the EIS responses against the logarithm of different concentrations of cells. The RCT increased with increasing Raji cell concentration.

https://dx.doi.org/10.1021/acs.analchem.0c02357
Anal. Chem. 2020, 92, 11405−11412

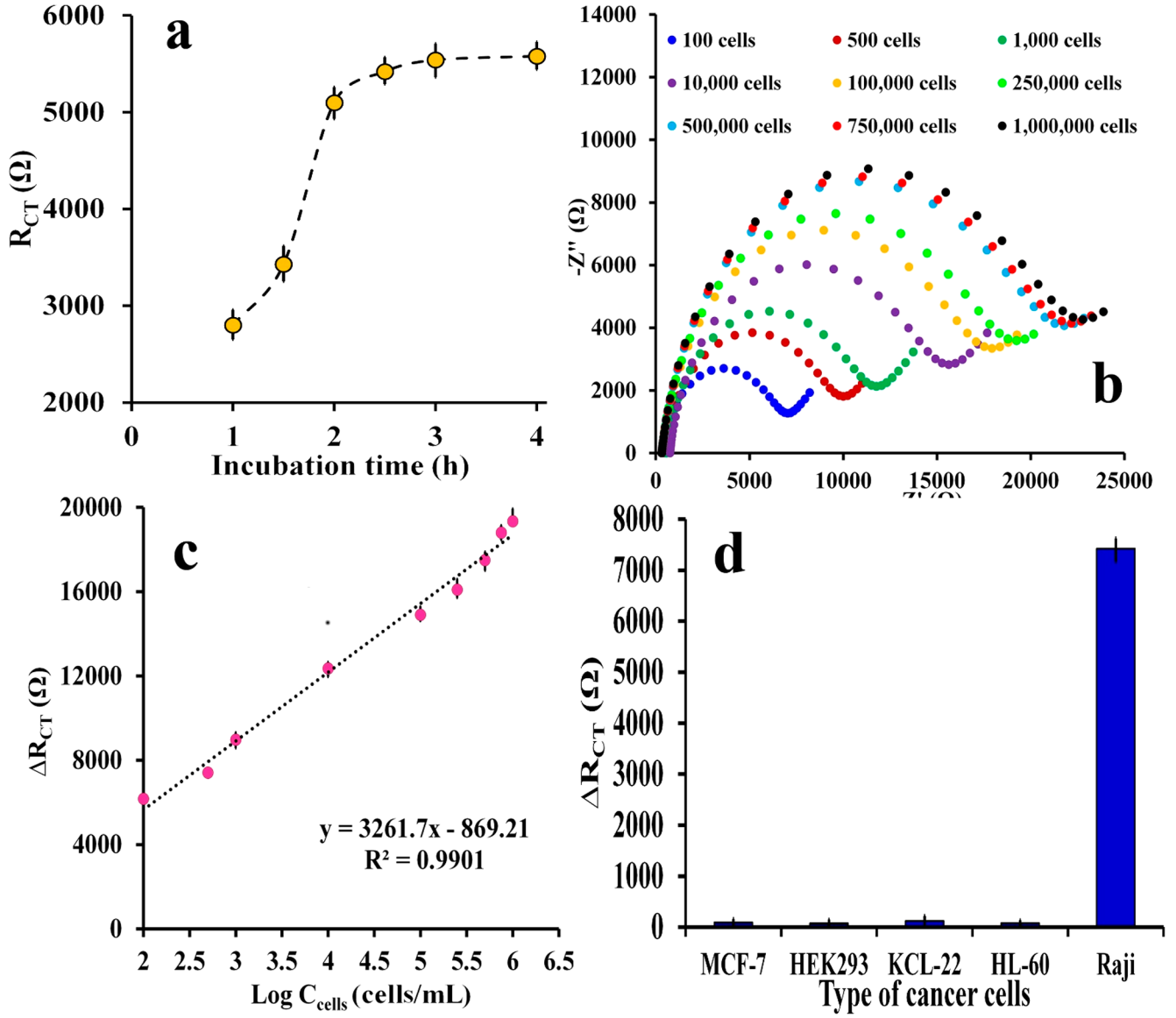

Figure 4. (a) Effect of the immunoreaction time (C_{cells} = 500 cell/mL). (b) Immunosensor Nyquist plots incubated with different Raji cell concentrations (100, 500, 1000, 10 000, 100 000, 250 000, 500 000, 750 000, 1 000 000 cells/mL). (c) Impedimetric immunosensor calibration curve for Raji cell detection (ΔR_{CT} vs log C). (d) Comparison of Raji cells (500 cells/mL) with MCF-7, HEK293, HL-60, and KCL-22 control cancer cells (1000 cells/mL).

Changes in RCT parameters were investigated and calculated using the following equation:[16]

$$\Delta R_{CT} = R_{CT(MGNR/BA/Ab/BSA/Rajicell)} - R_{CT(MGNR/BA/Ab/BSA)}$$

where $R_{CT(MGNR/BA/Ab/BSA/Rajicell)}$ is the value of the resistance when cancer cells are incubated with immobilized Ab, and $R_{CT\ (MGNR/BA/Ab/BSA)}$ is the resistance of the proposed immunosensor after blocking by BSA. As shown in Figure 4c, the relationship of the ΔR_{CT} and the logarithmic value of the concentration of the cells was well fitted by a linear regression with the equation $\Delta R_{CT} = 3261.7 \times \log C_{cells}$ (cells/mL) − 869.21 (R^2 = 0.9901) in the range from 100 to 1 000 000 cells/mL. The LOD for the suggested immunosensor was determined to be 38 cells/mL (based on $3S_b/m$).

A unique feature of the sensor is its reproducibility.[32] The response of the three fabricated sensors under the same conditions was evaluated for the detection of 500 cells/mL, and a relative standard deviation (RSD) of 2.7% was obtained. These results demonstrate that the proposed immunosensor has suitable reproducibility for the detection of Burkitt's lymphoma cells. To assess the storage stability of the immunosensor, the proposed immunoprobe was stored in PBS (pH 7.4) at 4 °C. After 7 days, the immunosensor response to the same cell counts had decreased by 4.2%, indicating that the immunosensor has positive stability.

Control Experiments. The detection of the target analyte in its natural environment, surrounded by interfering molecules, is one of the main challenges of biosensors.[35] To investigate the ability of the biosensor to selectively bind to target cancer cells, the immunosensor was exposed to four control human cells, including a breast cancer cell line (MCF-7), two leukemia cell lines (HL-60, KCL-22), one type of normal cell—human embryonic kidney (HEK293), and the test Raji cells. When the fabricated immunosensor was

https://dx.doi.org/10.1021/acs.analchem.0c02357
Anal. Chem. 2020, 92, 11405−11412

incubated with 1000 cells/mL of the control cells, the ΔR_{CT} value changed slightly. However, when the number of cells was decreased to 500 cells/mL, the R_{CT} increased dramatically. The results from the control experiments showed negligible binding of other cancer cells compared to Raji cells, confirming that the immunosensor has excellent selectivity for lymphoma cancer cells (see Figure 4d).

The electrochemical performance of the immunoprobe in the absence of BA (to Ab immobilization) was evaluated for the determination of cancer cells. In addition, the obtained EIS data were compared with the data in the presence of BA. The obtained calibration curves are shown in Figure S4. The plot of ΔR_{CT} as a function of log C_{cells} fitted into a linear equation of ΔR_{CT} = 1286.4 × log C_{cells} (cells/mL) − 940.28 with R^2 = 0.9934. The linear range and limit of detection for Raji cell determination by the MGNR/Ab/BSA immunosensor were 500−750 000 and 215 cells/mL, respectively.

To compare the performance of the SPCE/MGNR/BA/Ab/BSA and SPCE/MGNR/Ab/BSA immunosensors, the obtained calibration curves were investigated. For the MGNR/BA/Ab/BSA immunoprobe, the calibration curve slope was 3261.7, while for MGNR/Ab/BSA, it was 1286.4. Obviously, the sensitivity of the immunosensors is improved by the use of BA. It was also observed that for the MGNRs/BA/Ab/BSA immunoprobe, the linear range was wider and the detection limit lower than that of the MGNRs/Ab/BSA immune probe. These results prove that the proposed assay performance for the determination of cancer cells was improved in the presence of BA.

Evaluation of MGNR/BA Cytotoxicity. The details of this section are described in the Supporting Information

Real Sample Analysis. To evaluate the analytical applicability of the developed method, it is very significant and essential to detect the analyte in complex systems.[33] Elucidating the quantity of circulating tumor cells (CTCs), which can be produced during the early stages of tumorigenesis, in the peripheral blood or bone marrow can serve as an indicator for the clinical management of several cancer-related diseases by providing information on the success/failure of therapeutic intervention and disease stage forecasting. Here, human blood samples were evaluated as a complex systems model, and Raji cells were analyzed as one type of CTC in blood samples. Two different blood sample solutions were analyzed by the suggested method. The obtained results are shown in Table 2. Additionally, to evaluate the accuracy of the fabricated immunosensor, a comparative study of our proposed method and a conventional flow cytometry method was performed. The obtained results show good agreement between the two methods without significant differences (for confidence limits of 95%). This indicates that the proposed immunosensor is a promising approach for B lymphocyte lymphoma assays in blood samples without the significant matrix effect of the real sample. Also, in regard to the evaluation that blood proteins can have effect on the Raji cell measurements or not, two different concentrations of Raji cells (1000 and 100 000 cells/mL) were spiked to a healthy whole blood sample (without any Raji cells), and the obtained results were compared to an equivalent amount in the buffer. The errors were less than 5%. Obtained results are shown in Figure S6. Thus, immunosensors are especially suitable for the early diagnosis of B cell non-Hodgkin's lymphoma.

Table 2. Raji Cells Detected in Blood Samples by the Proposed Immunosensor and Conventional Flow Cytometry Method

sample	spiked (cells/mL)	found (cells/mL)	flow cytometry method (cells/mL)
patient blood sample 1	0	410	380
patient blood sample 2	0	560	510

CONCLUSIONS

This paper presents an effective signal amplification strategy for the ultrasensitive detection of lymphoma cancer cells based on the direct immobilization of well-oriented antibodies onto magnetic graphene nanoribbon-BA. The immobilization of antibodies plays an important role in immune-sensing applications. In this work, BA was used for proper Ab immobilization via N-glycans in the Fc region of Ab that is far from its binding sites. Since the N-glycans are quite far from the bottom (C-terminus) of Ab, if BA is directly attached to the electrode surface (without a spacer) or with a short spacer, Ab immobilization will not be achieved accurately. As a result, Ab binding sites for antigens are not optimal. To obtain well-oriented Ab with conformational freedom, the surface electrode is not covalently modified with BA, and BA is instead directly attached to the magnetic nanoparticle surfaces for the first time. With the dropping of modified nanoparticles into the Ab solution, BA can easily interact with Fc regions without the need for spacers. By the magnetic entrapment method (using the external magnetic field for the collection of magnetic nanocomposites on the working electrode in a homemade electrochemical cell), we were able use the SPCE multiple times without covalent modification of the electrode surface to characterize the electrolyte and sample small volumes. Additionally, this method leads to the elimination of many species interferences in real environmental analysis and can obtain accurate responses without the need for any real sample preparation method. This work presents a label-free immunosensor for lymphoma cancer cell determination in the concentration range of 100−1 000 000 cells/mL with an excellent detection limit (38 cells/mL), stability, reproducibility, and applicability in real samples.

ASSOCIATED CONTENT

Supporting Information

The Supporting Information is available free of charge at https://pubs.acs.org/doi/10.1021/acs.analchem.0c02357.

Reagents; instrumentation; preparation of GNR, MGNRs, MGNR/BA, and MGNR/BA/Ab; cell culture; MTT assay; characterization of the GNRs and MGNRs; characterization of the magnetic immunoprobe surfaces; evaluation of MGNR/BA cytotoxicity; and Figures S1−S7 (PDF)

AUTHOR INFORMATION

Corresponding Author

Hasan Bagheri − *Chemical Injuries Research Center, Systems Biology and Poisonings Institute, Baqiyatallah University of Medical Sciences, Tehran, Iran;* orcid.org/0000-0003-2895-6189; Email: h.bagheri@bmsu.ac.ir, h.bagheri82@gmail.com

https://dx.doi.org/10.1021/acs.analchem.0c02357
Anal. Chem. 2020, 92, 11405−11412

Authors

Pegah Hashemi − *Faculty of Chemistry, Bu-Ali Sina University, Hamedan, Iran*

Abbas Afkhami − *Faculty of Chemistry, Bu-Ali Sina University, Hamedan, Iran;* orcid.org/0000-0002-3559-2080

Behzad Baradaran − *Immunology Research Center, Tabriz University of Medical Sciences, Tabriz, Iran*

Raheleh Halabian − *Applied Microbiology Research Center, Systems Biology and Poisonings Institute, Baqiyatallah University of Medical Sciences, Tehran, Iran*

Tayyebeh Madrakian − *Faculty of Chemistry, Bu-Ali Sina University, Hamedan, Iran;* orcid.org/0000-0002-6876-7633

Fabiana Arduini − *Department of Chemical Science and Technologies, University of Rome Tor Vergata, 00133 Rome, Italy*

Tien Anh Nguyen − *Department of Physics, Le Quy Don Technical University, Ha Noi, Viet Nam*

Complete contact information is available at: https://pubs.acs.org/10.1021/acs.analchem.0c02357

Author Contributions

The manuscript was written through the contributions of all authors. All authors have given approval to the final version of the manuscript.

Notes

The authors declare no competing financial interest.

■ ACKNOWLEDGMENTS

The authors would like to thank the Research Council of Bu-Ali Sina University for the financial support of this work. Additionally, this research is funded by the Vietnam National Foundation for Science and Technology Development (NAFOSTED) under grant number 103.99-2017.65.

■ REFERENCES

(1) Wang, L.; Xiong, Q.; Xiao, F.; Duan, H. *Biosens. Bioelectron.* **2017**, *89*, 136−151.
(2) Tan, L.; Lin, P.; Chisti, M. M.; Rehman, A.; Zeng, X. *Anal. Chem.* **2013**, *85*, 8543−8551.
(3) Johnson, N. A.; Boyle, M.; Bashashati, A.; Leach, S.; Brooks-Wilson, A.; Sehn, L. H.; Chhanabhai, M.; Brinkman, R. R.; Connors, J. M.; Weng, A. P.; Gascoyne, R. D. *Blood* **2009**, *113*, 3773−3780.
(4) Maloney, D. G. *N. Engl. J. Med.* **2012**, *366*, 2008−2016.
(5) Shan, D.; Ledbetter, J. A.; Press, O. W. *Blood* **1998**, *91*, 1644−1652.
(6) Saaiq, M.; Siddiqui, S. *Burns* **2016**, *42*, 1143.
(7) Wang, L.; Abbasi, F.; Gaigalas, A. K.; Vogt, R. F.; Marti, G. E. *Cytometry, Part B* **2006**, *70*, 410−415.
(8) Chu, P. G.; Loera, S.; Huang, Q.; Weiss, L. M. *Am. J. Clin. Pathol.* **2006**, *126*, 534−544.
(9) Lim, S. H.; Beers, S. A.; French, R. R.; Johnson, P. W.; Glennie, M. J.; Cragg, M. S. *Haematologica* **2010**, *95*, 135−143.
(10) Ding, C.; Ge, Y.; Zhang, S. *Chem. - Eur. J.* **2010**, *16*, 10707−10714.
(11) Leo, N.; Shang, Y.; Yu, J.-J.; Zeng, X. *Langmuir* **2015**, *31*, 13764−13772.
(12) Xia, N.; Wang, X.; Yu, J.; Wu, Y.; Cheng, S.; Xing, Y.; Liu, L. *Sens. Actuators, B* **2017**, *239*, 834−840.
(13) Song, L.; Zhao, J.; Luan, S.; Ma, J.; Liu, J.; Xu, X.; Yin, J. *ACS Appl. Mater. Interfaces* **2013**, *5*, 13207−13215.
(14) Adak, A. K.; Li, B.-Y.; Huang, L.-D.; Lin, T.-W.; Chang, T.-C.; Hwang, K. C.; Lin, C.-C. *ACS Appl. Mater. Interfaces* **2014**, *6*, 10452−10460.
(15) Duval, F.; van Beek, T. A.; Zuilhof, H. *Analyst* **2015**, *140*, 6467−6472.
(16) Afkhami, A.; Hashemi, P.; Bagheri, H.; Salimian, J.; Ahmadi, A.; Madrakian, T. *Biosens. Bioelectron.* **2017**, *93*, 124−131.
(17) He, J.-J.; Yan, X.-H.; Guo, Y.-D.; Liu, C.-S.; Xiao, Y.; Meng, L. *Solid State Commun.* **2016**, *227*, 28−32.
(18) Higginbotham, A. L.; Kosynkin, D. V.; Sinitskii, A.; Sun, Z.; Tour, J. M. *ACS Nano* **2010**, *4*, 2059−2069.
(19) Nadiv, R.; Shtein, M.; Buzaglo, M.; Peretz-Damari, S.; Kovalchuk, A.; Wang, T.; Tour, J. M.; Regev, O. *Carbon* **2016**, *99*, 444−450.
(20) Shcherbakova, D. M.; Subach, O. M.; Verkhusha, V. V. *Angew. Chem., Int. Ed.* **2012**, *51*, 10724−10738.
(21) Chandra, V.; Park, J.; Chun, Y.; Lee, J. W.; Hwang, I.-C.; Kim, K. S. *ACS Nano* **2010**, *4*, 3979−3986.
(22) Hashemi, P.; Bagheri, H.; Afkhami, A.; Amidi, S.; Madrakian, T. *Talanta* **2018**, *176*, 350−359.
(23) Hashemi, P.; Bagheri, H.; Afkhami, A.; Ardakani, Y. H.; Madrakian, T. *Anal. Chim. Acta* **2017**, *996*, 10−19.
(24) Sheng, W.; Chen, T.; Kamath, R.; Xiong, X.; Tan, W.; Fan, Z. H. *Anal. Chem.* **2012**, *84*, 4199−4206.
(25) Chen, P.-C.; Wan, L.-S.; Ke, B.-B.; Xu, Z.-K. *Langmuir* **2011**, *27*, 12597−12605.
(26) Ivanov, A. E.; Kumar, A.; Nilsang, S.; Aguilar, M.-R.; Mikhalovska, L. I.; Savina, I. N.; Nilsson, L.; Scheblykin, I. G.; Kuzimenkova, M. V.; Galaev, I. Y. *Colloids Surf., B* **2010**, *75*, 510−519.
(27) Pelton, R.; Cui, Y.; Zhang, D.; Chen, Y.; Thompson, K. L.; Armes, S. P.; Brook, M. A. *Langmuir* **2013**, *29*, 594−598.
(28) Ahmadi, M.; Madrakian, T.; Afkhami, A. *Anal. Chim. Acta* **2014**, *852*, 250−256.
(29) Felix, F. S.; Angnes, L. *Biosens. Bioelectron.* **2018**, *102*, 470−478.
(30) Hashemi, P.; Afkhami, A.; Bagheri, H.; Amidi, S.; Madrakian, T. *Anal. Chim. Acta* **2017**, *984*, 185−192.
(31) Palomar, Q.; Gondran, C.; Holzinger, M.; Marks, R.; Cosnier, S. *Biosens. Bioelectron.* **2017**, *97*, 177−183.
(32) Kashefi-Kheyrabadi, L.; Mehrgardi, M. A.; Wiechec, E.; Turner, A. P.; Tiwari, A. *Anal. Chem.* **2014**, *86*, 4956−4960.
(33) Li, J.; Yan, X.; Li, X.; Zhang, X.; Chen, J. *Talanta* **2018**, *179*, 726−733.
(34) Liang, Y.; Huang, X.; Yu, R.; Zhou, Y.; Xiong, Y. *Anal. Chim. Acta* **2016**, *936*, 195−201.
(35) Urmann, K.; Arshavsky-Graham, S.; Walter, J.-G.; Scheper, T.; Segal, E. *Analyst* **2016**, *141*, 5432−5440.